BFUT P14

The Spaticle Field as the Unified Substrate of Physical Reality

A Cross-Programme Synthesis of Convergent Evidence, From Cosmology and Particle Masses to Consciousness

Vijay Shankar Sharma

Independent Researcher, Gurugram, National Capital Region, India

ORCID: 0009-0001-9622-6121 | vss@vijayshankarsharma.com

DOI: 10.5281/zenodo.19394064

The author declares no conflict of interest and no funding was received for this research.

Abstract

The Big Flare-Up Theory (BFUT) uses the Spaticle field as the physical matter substrate underlying results developed across its cosmological, gravitational, particle, quantum, relativistic, atomic, extreme-gravity, and sensing-channel papers. This paper is a synthesis only: it introduces no new equation, derivation, numerical result, mechanism, prediction, or statistical claim. Its quantitative starting point is the complete P16 particle-sector derivation of the equilibrium Spaticle-field density. P16 first obtains the dimensionless condensation minimum $R_0 = 1.27348221$ from $E(R) = A/R^2 + BR^2 + CR + D/R$ with $A = 0.5$, $B = 0.56308$, $C = -1/3$, and $D = 1$. The measured proton radius and mass then set the physical length and mass anchors; the chain proceeds through l_model, ħ_vss, m_e_vss, α_vss, the characteristic mass m_e/α, the classical-electron-radius scale r_e, and the particle-sector gravitational self-energy density u_g. The closure $\rho_s c^2 = u_g$ gives $\rho_s = 7.30294170 \times 10^{-27}$ kg m^{-3}, adopted as 7.3×10^{-27} kg m^{-3}. The remainder of the paper traces how this substrate, its density, and quantities derived from the same BFUT framework are used in the source papers: cosmological interpretation; matter and antimatter condensation; the emergence of fundamental interactions; finite-domain gravitation and Dark Matter Effects; SPARC and KiDS-1000 tests; particle resonances and constants; quantum-mechanical interpretation; time and relativistic effects; light, photons and gravitational-wave propagation; atomic structure and matter stability; finite-density compact objects; and the sensing-channel and consciousness framework. The two appendices reproduce the current cross-sector validation and the 106-item applications catalogue. All equations, mechanisms, numerical results, and interpretations summarised here remain attributable to their source papers.

Keywords: Spaticle field; physical substrate; substrate density; condensation; gravity; dark matter effects; particle physics; quantum mechanics; time; light; black holes; consciousness

1. Scope and Provenance Boundary

This paper does not establish an additional BFUT result. Its function is to collect, organise, and connect statements already made in the cited BFUT papers. Where a quantity is derived in one paper and used in another, the derivation remains attributed to that source. The equilibrium substrate density is derived once in the P16 particle-sector chain; later sectors use $\rho_s = 7.3 \times 10^{-27}$ kg/m³, or quantities derived from it, as applications, extensions, consistency checks, or observational tests rather than as independent derivations of ρ_s [P16, P18, P19, P25, P78].

Across the programme, the Spaticle field is described as a continuous physical matter substrate in which matter condenses and remains embedded and through which gravitational, electromagnetic, and other physical disturbances are organised or propagated [P16, P17, P18, P23]. The synthesis below therefore begins with the complete P16 density chain before following the field into the later papers.

2. P16 Derivation Chain of the Spaticle-Field Density

P16 states explicitly that the dimensionless coefficients A, B, C and D determine the equilibrium radius R_0, not ρ_s directly. The physical density appears only after the dimensionless condensation minimum is connected to the particle sector through measured proton anchors and the BFUT particle relations, and after the particle-sector gravitational energy-density scale is identified with the equilibrium substrate rest-energy density.

Step 1. Dimensionless condensation equilibrium: $A = 0.5$, $B = 0.56308$, $C = -1/3$, $D = 1$; $E(R) = A/R^2 + BR^2 + CR + D/R$; $R_0 = 1.27348221$. P16 verifies that the positive stationary radius is a minimum through $d^2E/dR^2 = 6A/R^4 + 2B + 2D/R^3 > 0$ for $R > 0$.

Step 2. Measured proton anchors and physical length: $r_p = 0.8414 \times 10^{-15}$ m and $m_p = 1.67262192369 \times 10^{-27}$ kg. The physical length represented by one model-radius unit is $l\_model = r_p/R_0 = 6.60708091 \times 10^{-16}$ m. P16 also uses c, e, ε_0 and G as supplied dimensional inputs.

Step 3. BFUT reduced Planck constant: $\hbar\_vss = m_p\, c\, l\_model/\pi = m_p\, c\, r_p/(\pi R_0) = 1.05457687 \times 10^{-34}$ J s.

Step 4. BFUT electron mass and fine-structure constant: $m\_e\_vss = m_p/(6\pi^5) = 9.10955518 \times 10^{-31}$ kg; $\alpha\_vss = e^2/(4\pi\varepsilon_0\hbar\_vss\, c) = 0.00729731763044$, giving $\alpha\_vss^{-1} = 137.036655199$. P16 specifies that the α value uses ħ_vss together with the supplied electromagnetic inputs e and ε_0.

Step 5. Characteristic particle mass and classical electron radius: $m\_e/\alpha = 1.24834297 \times 10^{-28}$ kg; $r\_e = \alpha\hbar\_vss/(m\_e\, c) = 2.81788728 \times 10^{-15}$ m. In these equations m_e and α denote the BFUT-calculated Step-4 values.

Step 6. Particle-sector gravitational self-energy density: $u\_g = G(m\_e/\alpha)^2/(8\pi r\_e^4) = 6.56355667 \times 10^{-10}$ J m^{-3}. P16 uses the positive gravitational energy-density prescription with the 8π normalisation and identifies $\rho_s c^2 = u\_g$ as the physical closure connecting the particle scale to the substrate.

Step 7. Equilibrium Spaticle-field mass density: $\rho_s = u\_g/c^2 = G(m\_e/\alpha)^2/(8\pi r\_e^4 c^2) = 7.30294170 \times 10^{-27}$ kg m^{-3}. P16 adopts the working value $\rho_s = 7.3 \times 10^{-27}$ kg m^{-3} and carries that value forward wherever ρ_s appears.

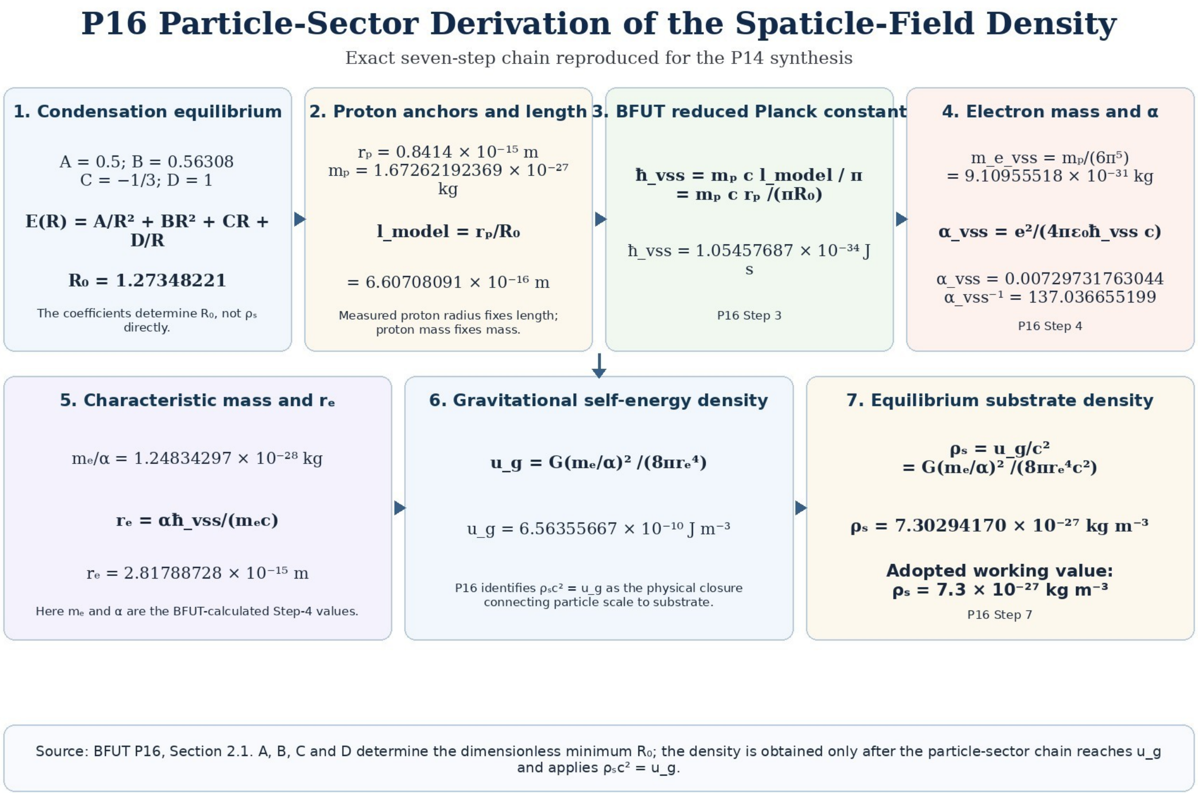

Figure 1. Complete P16 particle-sector derivation chain of the equilibrium Spaticle-field density. The coefficients A, B, C and D determine R_0; ρ_s is obtained only after the particle-sector chain reaches u_g and applies $\rho_s c^2 = u\_g$.

3. Cosmological Uses of the Spaticle-Field Framework

P1 treats the Hubble velocity-distance relationship as an emergent result of gravitational sorting rather than inserting metric expansion as the physical cause; its reported simulation gives a Pearson correlation r = 0.675 and 84% of surviving galaxies receding [P1]. P2 applies the one-substrate ontology to the cosmological-constant and QFT vacuum-energy problem. In the current P16 treatment, the corrected pure-vacuum empty-mode sum is u_QFT,corrected = 0, while the physical substrate has the separate finite rest-energy density $u_s = \rho_s c^2 = 6.56 \times 10^{-10}$ J/m³. P3 develops steady-state nucleosynthesis and the lithium problem, while P4 examines observer bulk flow as an alternative account of apparent cosmic acceleration [P2-P4].

P5 argues for spatial infinitude and no physical boundary [P5]. P6 treats black holes as gravitational vortices rather than physical infinite-density singularities [P6]. P7 gives the dynamic-thermal-equilibrium interpretation of the 2.725 K CMB temperature, and P8 reconstructs the long cold and dark stage preceding luminous structure [P7, P8]. P9 develops rotation and orbital hierarchy across scales [P9]. P10, P11, P12 and P13 respectively give substrate interpretations of the Sunyaev-Zel'dovich effect, the Lyman-alpha forest and absorption-percolation threshold, the integrated Sachs-Wolfe effect, and weak-lensing S8 results [P10-P13]. P15 separately addresses the state preceding matter and the Spaticle field and the sequence by which the substrate appears in the wider BFUT cosmology [P15].

4. Matter, Antimatter, and Stable Condensation

P16 develops the finite condensation framework from which stable matter structures are built. The condensation functional $E(R) = A/R^2 + BR^2 + CR + D/R$ has the interior minimum $R_0 = 1.27348221$ used in the density chain above. Matter is treated as organised condensation of the Spaticle field rather than as a substance separate from the substrate. P16 also gives the particle-scale relations $m\_e\_vss = m_p/(6\pi^5)$, $\hbar\_vss = m_p c r_p/(\pi R_0)$, $\alpha\_vss = e^2/(4\pi\varepsilon_0 \hbar\_vss\ c)$, and the particle-sector closure that yields ρ_s [P16].

P16A extends the construction to antimatter. It treats matter and antimatter as corresponding substrate condensation configurations, explains annihilation through cancellation of opposing organised excitations and release of condensation energy, and develops the stability filter governing which configurations persist. It also develops the antihydrogen comparison framework and the higher four-unit configuration excitations listed in Appendix B, including the Shankar and BFUT resonance assignments [P16A].

5. Fundamental Interactions and Gravitation

P17 derives the programme's stated sequence of gravity, strong, electromagnetic and weak interactions as distinct physical disturbance or organisation channels associated with the Spaticle substrate and the 3+e matter structure. It treats gravity as arising first from substrate deformation associated with condensation, followed by the strong interaction within the bound structure, electromagnetic behaviour from charge/counter-rotation organisation, and the weak interaction in the corresponding transition structure. The same paper subsequently uses these four interactions as the programme's fundamental sensing channels [P17].

P18 formulates gravitation through the covariant carrier-field equation F1-cov, substrate deformation, finite deformation domains and the Dark Matter Effects framework. Its density-derived inverse-length scale is $\mu_s = \sqrt{(3G\rho_s/c^2)} = 4.03359 \times 10^{-27}\ m^{-1}$, and the corresponding acceleration scale is $a_s = c^2\mu_s/3 = c\sqrt{(G\rho_s/3)} = 1.2084 \times 10^{-10}\ m\ s^{-2}$. The finite deformation-domain relation is $R\_d = (3M/8\pi\rho_s)$^(1/3). P18 states that F1-cov is the general carrier equation, while the organised galactic and lensing-stack regimes use the DME equation [P18].

6. Galactic Dynamics, Weak Lensing, and Dark-Matter Effects

P18, P25 and P78 apply the substrate-derived gravitational framework to the extra gravitational support conventionally attributed to dark matter. In the organised regime, the DME relation is $v^2(R) = v\_b^2(R)[1 + a_s R/v\_b^2(R)]$^(1/2), equivalently $g\_DME = g\_b[1 + a_s/g\_b]$^(1/2). The equation uses the baryonic distribution together with the single density-derived scale a_s rather than introducing a dark-matter particle or a per-galaxy fitted acceleration constant [P18, P25, P78].

The current validation record applies the same density-derived acceleration scale to 175 SPARC galaxies and to KiDS-1000 stacked weak-lensing bins. The cross-sector appendix records the SPARC shape agreement, flat/non-flat classification results and median outer residual, and identifies the KiDS-1000 stacks as a separate weak-lensing test using the same DME relation and density-derived scale. P14 reproduces those source-paper results in Appendix A rather than recalculating them.

7. Particle Physics and Fundamental Constants

P19 takes the P16 condensation geometry into the particle-physics closure programme. Among the source-paper relations reproduced in the current appendices are $m\_Z\_vss = \pi^4 m_p = 91.396$ GeV/c² and $m\_W\_vss = (256/3)m_p = 80.066$ GeV/c²; their ratio gives the stated on-shell electroweak quantity $\sin^2\theta\_W\_vss = 1 - (m\_W\_vss/m\_Z\_vss)^2 = 0.23257$. P19 also gives the strong-coupling expression $\alpha_s\_vss = BR_0^4/(8\pi A)$, the H-class radial-mode relation $\lambda\_H\_vss = 2AR_0/\pi^2$, and the resulting H-class mass $m\_H\_vss = 124.75$ GeV/c² [P19].

P16 and P19 connect the same condensation geometry to the action and electromagnetic scales. P16 gives ħ_vss = $1.05457687 \times 10^{-34}$ J s and $α\_vss^{-1}$ = 137.036655199 within the density chain above. P19 develops the corresponding particle-sector closure and resonance relations. P27 then rewrites standard quantum formulas and Planck-unit expressions using the BFUT action scale; those are downstream uses of the P16 result, not a second independent derivation of ħ [P16, P19, P27].

8. Quantum Mechanics and Quantum-Gravity Interpretation

P19A places quantum phenomena and gravitation within the common substrate framework. Its stated interpretations include half-integer spin through 720-degree restoration topology, the Born rule through substrate deformation-energy density, wave-function collapse as physical state resolution under interaction, and substrate accounts of superposition, entanglement, tunnelling, decoherence, Pauli exclusion, spin-statistics and gauge structures [P19A].

P19A also connects the covariant substrate carrier framework to the Schrödinger equation in the non-relativistic limit, so the standard wave equation is retained while the paper supplies a proposed physical substrate interpretation. P27 expresses Compton and de Broglie wavelengths, harmonic-oscillator levels, uncertainty relations and Planck units using ħ_vss. P24 applies the same substrate/action framework to quantum-computing questions including gate evolution, minimum gate time, substrate memory and quantum-correlation treatments [P19A, P24, P27].

9. Time, Light, Photons, and the Universal Speed Limit

P22 defines time as accumulated substrate evolution and develops special-relativistic and gravitational time dilation through allocation of finite substrate propagation capability. Its propagation-budget framework writes the available capacity in terms of spatial motion, internal evolution and gravitational deformation, and uses that same mechanism to discuss length contraction, the twin paradox, clock universality, the arrow of time, simultaneity and causality [P22].

P23 identifies c as the maximum rate at which the Spaticle substrate can reorganise and propagate a disturbance. It treats electric fields, magnetic fields and photons as bound and free dynamical states of organised electromagnetic excitation in the same substrate, and treats light and gravitational waves as sharing the same limiting propagation speed because both propagate through that substrate [P23]. The mechanical relation c_vss = $\sqrt{(K_s/\rho_s)}$ belongs to the source-paper substrate mechanics. Where K_s is written as $\rho_s c^2$, this form is a consistency identity; the separate numerical reconstruction of c is given in the particle/action chain [P19, P23, P27].

10. Atomic Structure and Matter Stability

P25 connects the substrate and particle-sector quantities to hydrogen ground-state structure, the Bohr radius, atomic stability and molecular or chemical stability. The current applications catalogue records these as downstream uses of ħ_vss, m_e_vss, α_vss and the corresponding atomic-energy relations. P16 also distinguishes these quantities from those that depend explicitly on ρ_s: a result is density-dependent only where ρ_s survives in its final displayed equation [P16, P19, P25, P27].

11. Finite-Density Extreme Gravity and Black Holes

P26 argues that finite substrate density, restoring dynamics and finite propagation capacity prevent physical infinite density and provide finite-density bounds for compact collapse [P26]. P28 develops the corresponding black-hole picture as a finite gravitational-vortex structure with a compressed core, surrounding redistribution and entrainment regions, rotational sustenance and a finite deformation domain. P6 supplies the earlier Universal Centrality Rule and gravitational-vortex treatment. P14 records these source-paper mechanisms without adding a new compact-object model [P6, P26, P28].

12. From Fundamental Interactions to Sensing and Consciousness

P17 treats the four fundamental interactions as a hierarchy of physical sensing channels as well as interactions. P20 develops the subsequent sensing-channel framework and its formal conditions for sensing, including the Hierarchical Channel Accessibility model. P21 develops the Consciousness Index as the programme's scalar measure of conscious degree, structure and evolutionary potential. P14 does not derive consciousness from the density equation; it only records the source papers' stated conceptual chain from physical substrate and interactions to sensing channels and then to the P20-P21 consciousness framework [P17, P20, P21].

P14 therefore stops at synthesis: it records the programme's stated chain from substrate to matter, from matter to interactions, from interactions to sensing channels, and from sensing channels to the consciousness framework. The definitions, derivations, and claims at each stage remain those of the cited source papers.

13. Conclusion

The Spaticle field is therefore not established by a single claim in P14 but by the roles assigned to it across the BFUT source papers. P16 supplies the complete particle-sector density derivation; P16A develops antimatter and the stability filter; P17 and P18 develop interactions, carrier gravitation, finite domains and DME; P19 and P19A develop particle closure and quantum interpretation; P22 and P23 develop time and propagation; P25-P28 and P78 apply the same framework to atomic structure, galaxy dynamics, weak lensing, the action scale, finite-density collapse and black holes; the cosmological papers apply the substrate ontology to their respective large-scale phenomena; and P20-P21 develop the sensing-channel and consciousness framework. The two appendices that follow reproduce the programme's current cross-sector validation and 106-item applications catalogue. No additional physical result is asserted in this synthesis.

Appendix A

Cross-Sector Validation of the Spaticle Field & Its Density

The Big Flare-Up Theory (BFUT) framework identifies the Spaticle Field as the physical substrate underlying the phenomena addressed across the programme. Its intrinsic equilibrium density is $\rho_s = 7.3 \times 10^{-27}$ kg/m³ derived from the free energy condensation functional.

The following sector-wise table brings together the physical domains in which the Spaticle Field, its density, and quantities derived from it provide relationships, quantitative results, or observational validation.

S. No.	Physical sector	Spaticle Field quantities used or derived	Validation / physical result	BFUT papers
1	Cosmology and large-scale structure	ρ_s; substrate energy density $u_s = \rho_s c^2$; gravitational domain scale derived from ρ_s	Cosmological vacuum-energy relationship; finite substrate gravitational domain; large-scale structure and related cosmological consequences addressed through the BFUT substrate framework.	P14, P18, P23, P25, P26, P27
2	Gravitation and gravitational field	ρ_s; carrier mass scale μ_s; L_s; acceleration scale a_s; substrate deformation	Covariant carrier equation, finite deformation-domain radius, dark matter effects equation (DME) gravitational response, and a unified gravitational description across quantum, classical, galactic, and rapid-transition regimes.	P17, P18, P25, P26
3	Galactic dynamics and dark-matter effects	ρ_s; $a_s = 1.208 \times 10^{-10}$ m/s²; DME equation; DDR domain	SPARC validation across 175 galaxies: 92.0% shape agreement, 98.8% flat classification, 14.3% non-flat classification, and median outer relative residual 0.096. DME accounts for the observed extra gravitational support without introducing a dark-matter particle.	P18, P25, P26, P78
4	Weak gravitational lensing	ρ_s; a_s; DME domain response	KiDS-1000 validation using the same DME relation and the same density-derived acceleration scale. The four stacked stellar-mass bins provide an independent weak-lensing test of the gravitational response.	P18, P25, P27, P78
5	Particle physics and fundamental constants	R_0; ħ_vss; m_e_vss; α_vss; α_s_vss; M; m_W_vss; m_Z_vss; sin²θ_W_vss; λ_H_vss; v_vss; m_H_vss; m_Shankar; m_BFUT	The P16 condensation geometry supplies the common particle-sector origin. P19 gives the independent resonances m_Z_vss = $\pi^4 m_p$ = 91.396 GeV/c² and m_W_vss = 256M = $(256/3)m_p$ = 80.066	P16, P16A, P17, P19, P19A, P25, P27

S. No.	Physical sector	Spaticle Field quantities used or derived	Validation / physical result	BFUT papers
			GeV/c²; their ratio gives $\sin^2\theta$_W_vss = 0.23257. The radial mode gives λ_H_vss = $2AR_0/\pi^2$ and m_H_vss = 124.75 GeV/c². P16A gives the higher four-unit configuration excitations m_Shankar c² = 776.5 MeV (2+2) and m_BFUT c² = 1403.7 MeV (4+0).	
6	Quantum mechanics	ρ_s; condensation structure; ℏ; particle mass relations	BFUT P19A connects the substrate-based particle structure with quantum phenomena including half-integer spin, the Born rule, wave-function collapse, and Higgs physics, within the unified quantum-gravity framework.	P16, P19A, P25, P27
7	Atomic physics and matter stability	ρ_s; ħ_vss; m_e_vss; α_vss; a_0_vss; E_H_vss	Hydrogen ground-state and Bohr-radius results follow from ħ_vss, m_e_vss and α_vss. Matter stability follows from the corresponding atomic-scale and bond-energy relations.	P16, P19, P25, P27
8	Light, photons, and gravitational-wave propagation	ρ_s; substrate stiffness K_s; c	Photon and gravitational-wave propagation arise from the same substrate propagation mechanism. The universal speed limit is written mechanically as c_vss = $\sqrt{(K_s/\rho_s)}$, with an independent numerical reconstruction of c_vss from the BFUT quantity chain.	P17, P18, P19, P23, P25
9	Time and relativity	ρ_s; c; substrate propagation efficiency η; carrier response structure	Time is treated as accumulated substrate evolution. Kinematic and gravitational time dilation arise from the allocation of finite substrate propagation capability between spatial motion, internal evolution, and gravitational deformation.	P18, P19, P22, P23
10	Extreme gravity, singularity limits, and black holes	ρ_s; substrate deformation and finite-density dynamics; gravitational-vortex structure	Physical substrate dynamics impose a finite-density causal bound and remove the need to interpret infinite density as a physical state. Black holes are treated as gravitational vortices, with the Universal Centrality Rule providing an observational structural test.	P6, P26, P28

Appendix B

Applications and Derived Results of the Spaticle Field

This appendix lists independently meaningful physical applications, derived results, predictions, and observational applications that have a direct derivational or physical chain to the Spaticle Field or its derived density. Intermediate mathematical calculations are not listed as separate applications.

SN	Application / Derived Result	Physical result or BFUT application	BFUT source
1	Spaticle-field equilibrium density	Intrinsic substrate density ρ_s = 7.3×10^{-27} kg/m³, obtained from the condensation framework and used as the common physical substrate parameter.	P16; P25; P78
2	Matter creation from the Spaticle Field	Matter condenses from the physical Spaticle Field and remains embedded in it. This provides the substrate basis for the particle and matter structures developed throughout BFUT.	P14; P16; P17
3	Propagation of forces and physical disturbances through the Spaticle Field	Forces and physical disturbances propagate through the Spaticle Field. This supplies the common physical carrier underlying the electromagnetic, gravitational, weak, and strong interaction descriptions.	P14; P17; P18; P23
4	Stable condensation equilibrium	The condensation functional produces a finite non-zero equilibrium condensation scale R_0 for stable matter structures.	P16
5	Proton condensation structure	The three-core condensation architecture produces the structural basis for proton formation.	P16
6	3+e proton structure	The stable 3+e organisation supplies the particle architecture used in the proton and electron formation chain.	P16; P17
7	Electron mass	The BFUT particle chain derives electron mass from the proton-scale condensation construction.	P16; P19
8	Matter-antimatter structure and annihilation	Matter and antimatter are treated as corresponding substrate condensation configurations, with annihilation arising from cancellation of opposing organised excitations and release of condensation energy.	P16; P16A
9	Antihydrogen structure and CERN comparison	The BFUT antimatter construction gives a mirror configuration for antihydrogen and provides a framework for comparison with CERN antihydrogen measurements.	P16A
10	Stability filter for matter and antimatter	The stability filter identifies which condensation configurations can persist as stable matter or antimatter	P16; P16A

SN	Application / Derived Result	Physical result or BFUT application	BFUT source
		structures.	
11	Emergence of the fundamental forces	Gravity, strong, electromagnetic, and weak interactions are derived as distinct physical disturbance or organisation channels associated with the substrate and 3+e matter structure.	P17
12	Gravity as substrate deformation and restoring response	Gravitational attraction is described as the restoring response of the Spaticle Field to matter-induced deformation.	P17; P18
13	Covariant carrier-field equation	F1-cov provides the covariant substrate equation governing gravitational deformation and propagation.	P18
14	Density-derived carrier scale	The substrate density fixes the carrier scale μ_s and its associated propagation/screening scales.	P18
15	Finite gravitational deformation domain	For source mass M, BFUT gives a finite deformation-domain radius R_d = [3M/(8πρ$_s$)]^(1/3).	P18; P22; P26
16	Rotationally enlarged deformation domain	The effective deformation domain incorporates the rotational correction defined by the BFUT carrier model.	P18
17	Carrier relaxation length and timescale	The carrier framework supplies finite response and relaxation scales for substrate deformation.	P18; P26
18	Cosmological screening length	The density-derived carrier mass establishes a finite cosmological screening scale for the static carrier field.	P18
19	BFUT gravitational acceleration scale	The characteristic acceleration a_s is derived from the substrate density, G, and c.	P18; P78
20	Finite-domain gravity across physical regimes	The finite deformation-domain carrier is formulated for quantum, classical, galactic, and rapid-transition regimes, providing a common and testable gravitational description across those scales.	P18
21	Dark Matter Effects interpretation	The gravitational effect conventionally attributed to dark matter is represented in BFUT by organised or entrained Spaticle-field structure.	P18; P25; P78
22	Dark Matter Effects equation	The DME relation derives the additional rotational contribution from the baryonic distribution and the substrate-derived acceleration scale without modifying Newtonian gravity.	P18; P25; P78
23	SPARC rotation-curve validation	DME is applied to the 175-galaxy SPARC sample using the same substrate-derived acceleration scale and published baryonic inputs.	P25; P78

SN	Application / Derived Result	Physical result or BFUT application	BFUT source
24	KiDS-1000 weak-lensing validation	DME is applied to the KiDS-1000 stacked weak-lensing mass bins using the same substrate-derived acceleration scale.	P25; P78
25	Additional galaxy-system tests	DME is tested against additional named systems, including low-dark-matter and ultra-diffuse systems in the observational programme.	P25; P78
26	Merger morphology and substrate entrainment	Merger systems are interpreted through the redistribution and entrainment of substrate-associated mass during interaction.	P78
27	Low-rotation systems	Systems with negligible organised rotation provide a regime in which the substrate contribution predicted by the rotational DME mechanism is correspondingly reduced.	P25; P78
28	Sunyaev-Zel'dovich effect	P10 gives a Spaticle-field interpretation of the SZ effect through interaction of propagating substrate modes with the thermal electron population.	P10; P25
29	Lyman-alpha forest	P11 interprets the Lyman-alpha absorption forest through the interaction of propagating structures with the substrate and the absorption-percolation threshold.	P11; P25
30	Integrated Sachs-Wolfe effect	P12 attributes the ISW temperature contribution to variations in Spaticle-field density encountered by photons along their path.	P12; P25
31	Weak-lensing S8 application	P13 connects the weak-lensing S8 result and suppressed late-time structure growth to the physical substrate and its domain dynamics.	P13; P25
32	CMB acoustic peaks	The BFUT cosmological substrate framework models acoustic structure through ongoing shell processes in the physical substrate and reproduces CMB-like peak structure in the reported proof-of-principle treatment.	P12; P25
33	BAO-like feature	The same cosmological substrate treatment produces a BAO-like feature in the reported proof-of-principle simulation.	P12; P25
34	Fine-structure constant	The fine-structure constant α_vss is derived from the BFUT condensation and electromagnetic circulation structure.	P19; P27
35	Strong coupling constant	The strong coupling α_s_vss is derived from the P16 condensation parameters and evaluated at the Z-boson mass	P19

SN	Application / Derived Result	Physical result or BFUT application	BFUT source
		scale.	
36	Weak mixing angle	The BFUT electroweak mixing quantity is read from the independently derived resonance masses: $\sin^2\theta\_W\_vss = 1 - (m\_W\_vss/m\_Z\_vss)^2 = 0.23257$.	P19
37	W-boson mass	The charged W resonance is the n=4 coherent reconfiguration: $m\_W\_vss = 256M = (256/3)m_p = 80.066$ GeV/c². No mixing angle enters this mass relation.	P19; P25
38	Z-boson mass	The neutral Z core-stay resonance follows from the proton-scale condensation chain: $m\_Z\_vss = \pi^4 m_p = 91.396$ GeV/c². No mixing angle enters this mass relation.	P19; P25
39	H-class radial resonance mass	The radial H resonance follows from $\lambda\_H\_vss = 2AR_0/\pi^2$ and $v\_vss = 6E\_unit/\alpha\_vss$: $m\_H\_vss = v\_vss\sqrt{(2\lambda\_H\_vss)} = 124.75$ GeV/c².	P19
40	H-class state as a radial resonance	The observed H-class state is a radial resonance of the one Spaticle field; BFUT introduces no separate Higgs field.	P19A
41	Shankar and BFUT configuration resonances	P16A derives the 2+2 Shankar resonance at m_Shankar c² = 776.5 MeV and the 4+0 BFUT resonance at m_BFUT c² = 1403.7 MeV from the four-unit configuration gaps and E_unit.	P16A
42	Quark-mass hierarchy	The particle programme derives the quark-mass hierarchy from the condensation and circulation architecture.	P19; P19A
43	Hydrogen Bohr radius	BFUT-derived particle and action quantities are used in the atomic relation for the hydrogen ground-state radius.	P16; P25
44	Hydrogen ground-state binding energy	The BFUT atomic construction gives the hydrogen ground-state binding energy.	P16; P25
45	Atomic stability	The finite condensation structure and substrate density are connected to the persistence of atomic structure.	P25
46	Molecular and chemical stability	P25 derives sensitivity of atomic and molecular structure to the substrate density, including a density threshold associated with disruption of chemical bonding.	P25
47	Electron reference length	The electron reference length is an independently meaningful electromagnetic length scale used in the BFUT particle-sector construction and connected to the substrate-	P19; P78

SN	Application / Derived Result	Physical result or BFUT application	BFUT source
		derived particle parameters.	
48	Reduced Planck constant	The reduced Planck constant is derived from proton mass, proton charge radius, c, and the condensation minimum R_0: $\hbar$_vss = m_p c $r_p/(\pi R_0)$.	P16; P27
49	Planck constant	Planck's constant follows as h_vss = $2\pi\hbar$_vss and supplies the action quantum used in BFUT quantum relations.	P16; P27
50	Minimum circulation quantum	The minimum angular-momentum scale $\hbar$_vss/2 is connected to the 720° restoration topology of the matter condensation.	P19A; P27
51	Compton wavelength	The Compton wavelength is expressed using the BFUT action scale and particle parameters.	P27
52	de Broglie wavelength	The de Broglie wavelength is expressed using the BFUT action scale and particle momentum.	P27
53	Harmonic-oscillator energy levels	The harmonic-oscillator spectrum is expressed using the $\hbar$_vss and the corresponding quantum action scale.	P27
54	Planck length	The Planck length is derived from $\hbar$_vss together with G and c.	P27
55	Planck mass	The Planck mass is derived from $\hbar$_vss together with G and c.	P27
56	Planck time	The Planck time is derived from $\hbar$_vss together with G and c.	P27
57	Vacuum energy density	The equilibrium substrate rest-energy density is u_vac = $\rho_s c^2$.	P25; P27
58	Schrödinger equation	The time-dependent Schrödinger equation is derived as the non-relativistic limit of the covariant substrate carrier equation.	P19A; P27
59	Born rule	The Born probability $P(x)=\|\psi(x)\|^2$ is given a physical substrate interpretation through deformation-energy density and measurement interaction.	P19A
60	Heisenberg uncertainty principle	The uncertainty scale is connected to the finite localisation and action scale of substrate condensations.	P19A; P27
61	Half-integer spin	Half-integer spin is derived from the 720° restoration topology of the matter condensation.	P19A; P27
62	Spin-statistics relation	The distinction between embedded matter condensations and propagating substrate disturbances supplies the BFUT physical interpretation of fermionic and	P19A; P27

SN	Application / Derived Result	Physical result or BFUT application	BFUT source
		bosonic statistics.	
63	Pauli exclusion principle	Pauli exclusion is explained through the impossibility of identical fermionic condensations occupying one complete circulation state.	P19A; P27
64	Fermionic mass hierarchy	Fermionic mass structure is connected to organised circulation within the condensation architecture.	P19A
65	Gauge symmetry	U(1), SU(2), and SU(3) gauge structures are interpreted through local circulation invariance of substrate condensations.	P19A
66	Quantum superposition	Superposition is given a physical substrate interpretation as distributed organised excitation before interaction resolves the state.	P19A
67	Wave-function collapse	Wave-function collapse is interpreted as physical state resolution produced by interaction with matter in the substrate.	P19A
68	Entanglement	Entanglement is interpreted through shared coherent substrate structure and correlated physical states.	P19A
69	Quantum tunnelling	Tunnelling is represented through substrate condensation-boundary penetration, with the penetration scale determined by the BFUT action and barrier parameters.	P19A; P27
70	Decoherence	Decoherence is interpreted as loss of coherent substrate organisation through environmental interaction.	P19A
71	Quantum measurement	Measurement is treated as physical interaction between a quantum excitation and detector matter, providing the mechanism for state resolution.	P19A
72	Quantum gravity unification	Quantum behaviour and gravitation are placed within one substrate framework through the common carrier field and physical substrate.	P18; P19A
73	Quantum gate evolution	Quantum-gate unitary evolution is expressed using the BFUT-derived action scale, linking phase accumulation to substrate action.	P24; P27
74	Quantum-gate minimum time	The minimum controlled gate time is connected to the BFUT action scale and control-field energy.	P24; P27
75	Quantum-computing substrate memory	The P24 substrate-memory timescale is connected to the same substrate density that	P24; P27

SN	Application / Derived Result	Physical result or BFUT application	BFUT source
		fixes the BFUT action scale.	
76	Bell correlation	The Bell correlation function is connected to the Born rule and BFUT spin topology in the quantum-computing treatment.	P24
77	CHSH quantum bound	The BFUT quantum-computing treatment incorporates the quantum CHSH bound within its substrate interpretation of quantum correlations.	P24
78	Time as accumulated substrate evolution	Time is defined as accumulated evolution of physical states in the Spaticle substrate.	P22
79	Special-relativistic time dilation	Kinematic time dilation is derived from the finite propagation budget shared between spatial motion and internal evolution.	P22
80	Gravitational time dilation	Gravitational time dilation is derived from reduced local substrate propagation efficiency caused by gravitational deformation.	P22
81	Unified time-dilation relation	Kinematic and gravitational effects are combined through the common propagation-budget framework.	P22
82	Length contraction	Length contraction is derived as a second consequence of the same propagation-budget constraint.	P22
83	Twin paradox	The twin paradox is resolved through the different substrate propagation histories of the two clocks.	P22
84	Clock universality	All physical clocks slow by the same factor because physical clocks are substrate processes subject to the same propagation budget.	P22
85	Photon proper time	A photon assigns its full propagation budget to spatial propagation, giving zero proper time in the BFUT formulation.	P22; P23
86	Arrow of time	The direction of time is linked to irreversible outward substrate propagation and accumulated state change.	P22
87	Simultaneity and causality	Finite substrate propagation speed supplies the physical basis for causal ordering and simultaneity relations.	P22; P23
88	Past and future asymmetry	The substrate evolution framework provides a physical account of the distinction between completed and not-yet-completed state evolution.	P22
89	Quantum time evolution	Quantum time evolution is placed within the same physical substrate evolution that defines time macroscopically.	P22; P19A

SN	Application / Derived Result	Physical result or BFUT application	BFUT source
90	Equivalence principles	The weak, Einstein, and strong equivalence principles are examined within the BFUT substrate framework.	P22
91	Temporal singularity limit	Finite substrate propagation capacity supplies a temporal argument against physically reaching an infinite-density singularity.	P22; P26
92	Universal speed limit	c is identified as the maximum rate at which the Spaticle substrate can reorganise and propagate a disturbance.	P23
93	Speed of light from substrate stiffness and density	The propagation speed is derived as $c\_vss = \sqrt{(K\_s/\rho_s)}$.	P23
94	Independent reconstruction of c	The speed of light is reconstructed as c_vss, as a consistency relation of the ħ identity, from e, R_0, ε_0, m_p, r_p, and α_vss.	P19; P23; P27
95	Massive-particle velocity deficit	A massive condensation devotes part of its physical energy budget to internal structure, leaving less capacity for spatial propagation.	P23
96	Equality of light and gravitational-wave speeds	Light and gravitational waves are disturbances of the same substrate and therefore share the same limiting propagation speed.	P23
97	Singularity impossibility	Finite substrate density and restoring dynamics prevent physical infinite density.	P26
98	Finite-density causal bound	The causal bound $\bar{\rho}\_max = 3c^6/(4\pi G^3M^2)$ gives a finite mean-density limit for compact collapse.	P26
99	Finite gravitational compression	The substrate restoring mechanisms oppose unlimited gravitational compression.	P26; P28
100	Black holes as finite gravitational vortices	Black holes are represented as finite-density gravitational vortex structures without a physical infinite-density singularity.	P6; P26; P28
101	Black-hole finite core and surrounding structure	The BFUT black-hole model specifies a finite compressed core together with surrounding redistribution, coherence, and entrainment regions.	P28
102	Black-hole redistribution and entrainment	Organised deformation is redistributed from the compressed core into the surrounding shell and deformation domain.	P28
103	Black-hole deformation domain	The finite deformation-domain relation defines the outer extent of organised substrate deformation around a compact mass.	P18; P26; P28
104	Rotational sustenance of gravitational structure	Sustained rotation is treated as the dynamical condition	P26; P28

SN	Application / Derived Result	Physical result or BFUT application	BFUT source
		supporting organised gravitational-vortex structure and continued compression.	
105	Black-hole seed dissipation	The substrate relaxation framework supplies a characteristic dissipation timescale for transient deformation.	P26
106	Hawking-radiation interpretation	Within the finite-substrate black-hole structure, BFUT argues that Hawking radiation has no physical realisation.	P28

References

[P1] Sharma, V. S. (2026). Gravitational Sorting as an Alternative Mechanism for the Hubble Relationship. BFUT Paper 1. Zenodo. DOI: 10.5281/zenodo.19226423

[P2] Sharma, V. S. (2026). The Physical Identity of the Cosmological Constant. BFUT Paper 2. Zenodo. DOI: 10.5281/zenodo.19242083

[P3] Sharma, V. S. (2026). A Steady-State Nucleosynthesis Resolution of the Cosmological Lithium Problem. BFUT Paper 3. Zenodo. DOI: 10.5281/zenodo.19205920

[P4] Sharma, V. S. (2026). Observer Bulk Flow as an Alternative Explanation for Apparent Cosmic Acceleration. BFUT Paper 4. Zenodo. DOI: 10.5281/zenodo.19228065

[P5] Sharma, V. S. (2026). The Universe Has No Boundary: Logical, Derivational, and Observational Arguments for Spatial Infinitude. BFUT Paper 5. Zenodo. DOI: 10.5281/zenodo.19242759

[P6] Sharma, V. S. (2026). Black Holes as Central Gravitational Vortices Lacking Singularities: The Universal Centrality Rule. BFUT Paper 6. Zenodo. DOI: 10.5281/zenodo.19300874

[P7] Sharma, V. S. (2026). Dynamic Thermal Equilibrium as an Alternative Origin for the CMB Temperature. BFUT Paper 7. Zenodo. DOI: 10.5281/zenodo.19302025

[P8] Sharma, V. S. (2026). Cold, Dark, and Inevitable: A Logical Reconstruction of the Universe Before the Big Flare-Up. BFUT Paper 8. Zenodo. DOI: 10.5281/zenodo.19323579

[P9] Sharma, V. S. (2026). Cosmic Rotation Across Scales, Emergent Orbital Hierarchy, and the Large-Scale Challenge to Metric Expansion. BFUT Paper 9. Zenodo. DOI: 10.5281/zenodo.19341549

[P10] Sharma, V. S. (2026). The Sunyaev-Zel'dovich Effect as Local Substrate Interaction: A Big Flare-Up Theory Reinterpretation. BFUT Paper 10. Zenodo. DOI: 10.5281/zenodo.19377396

[P11] Sharma, V. S. (2026). The Lyman-Alpha Forest in the Big Flare-Up Theory: Absorption Percolation Threshold. BFUT Paper 11. Zenodo. DOI: 10.5281/zenodo.19383804

[P12] Sharma, V. S. (2026). The Integrated Sachs-Wolfe Effect in BFUT: Local Spaticle Field Temperature Variations as an Alternative Origin. BFUT Paper 12. Zenodo. DOI: 10.5281/zenodo.19391470

[P13] Sharma, V. S. (2026). Weak Gravitational Lensing and the S8 Tension in BFUT: Why Late-Time Clustering Inference Is Not a Unique Test of Lambda-CDM. BFUT Paper 13. Zenodo. DOI: 10.5281/zenodo.19392597

[P15] Sharma, V. S. (2026). What Existed Before Matter and the Spaticle Field: The Origin of Space, Time, and the Physical Substrate of Reality in an Infinite Universe. BFUT Paper 15. Zenodo. DOI: 10.5281/zenodo.19811691

[P16] Sharma, V. S. (2026). The Origin of Matter, Antimatter, and Fundamental Forces: How Protons, Electrons, and Hydrogen Formed. BFUT Paper 16. Zenodo. DOI: 10.5281/zenodo.19908215

[P16A] Sharma, V. S. (2026). Antimatter, Annihilation, and the Stability Filter: Predictions for the CERN Antihydrogen Programme. BFUT Paper 16A. Zenodo. DOI: 10.5281/zenodo.20201014

[P17] Sharma, V. S. (2026). The Emergence of Forces and Fundamental Senses: How the Spaticle Field Gave Rise to Gravity and All Other Forces. BFUT Paper 17. Zenodo. DOI: 10.5281/zenodo.19976408

[P18] Sharma, V. S. (2026). Beyond General Relativity: A Unified Gravitation Equation Across Quantum, Classical, Galactic, and Rapid-Transition Regimes. BFUT Paper 18. Zenodo. DOI: 10.5281/zenodo.20145506

[P19] Sharma, V. S. (2026). Unification of Particle Physics: Deriving Fine Structure and Coupling Constants, W, Z, and Higgs Boson Masses, Redefining and Unifying Gravity and Time. BFUT Paper 19. Zenodo. DOI: 10.5281/zenodo.20145567

[P19A] Sharma, V. S. (2026). Unifying Quantum Mechanics with Gravity, Demystifying Twenty Quantum Phenomena Including Half-Integer Spin, the Born Rule, Wave Function Collapse, and Higgs Physics. BFUT Paper 19A. Zenodo. DOI: 10.5281/zenodo.20145695

[P20] Sharma, V. S. (2026). From Matter and Fundamental Forces to Consciousness: A Unified Framework of Sensing Channels, Control, and Evolution. BFUT Paper 20. Zenodo. DOI: 10.5281/zenodo.19992457

[P21] Sharma, V. S. (2026). The Consciousness Index (CI): A Physically Grounded Scalar Measure of Conscious Degree, Structure, and Evolutionary Potential. BFUT Paper 21. Zenodo. DOI: 10.5281/zenodo.20025739

[P22] Sharma, V. S. (2026). Time: Identifying the Cause and Effects and Unifying General and Special Relativity. BFUT Paper 22. Zenodo. DOI: 10.5281/zenodo.20556908

[P23] Sharma, V. S. (2026). Light, Photons, and the Universal Speed Limit: A First-Principles Derivation of c from Substrate Condensation Dynamics. BFUT Paper 23. Zenodo. DOI: 10.5281/zenodo.20577935

[P24] Sharma, V. S. (2026). Quantum Computing and the Missing Physics Causing Delays and Overspend: Real Unknown Unknowns Identified Through the BFUT Substrate Framework. BFUT Paper 24. Zenodo. DOI: 10.5281/zenodo.20620192. Access to the full derivations and experimental proposals in this paper is restricted by the author.

[P25] Sharma, V. S. (2026). Dark Matter: Connecting Galaxy Clusters, Galaxy Rotations, the Cosmological Constant, W and Z Boson Masses, and Atomic Structure Through One Physical Constant. BFUT Paper 25. Zenodo. DOI: 10.5281/zenodo.20535295

[P26] Sharma, V. S. (2026). Singularity: Why and How Physical Substrate Dynamics Make Infinite Density Impossible. BFUT Paper 26. Zenodo. DOI: 10.5281/zenodo.20557070

[P27] Sharma, V. S. (2026). The Planck Constant: A First-Principles Derivation of ħ and How It Reshapes the Interpretation of Quantum Mechanics. BFUT Paper 27. Zenodo. DOI: 10.5281/zenodo.20620283

[P78] Sharma, V. S. (2026). Extra Gravity in SPARC and KiDS-1000 Without a Dark-Matter Particle or Changing Newtonian Gravity: The Connection to Electron Mass and the Fine-Structure Constant. BFUT Paper 78. Zenodo. DOI: 10.5281/zenodo.22696262

[P28] Sharma, V. S. (2026). Black Holes Demystified: What They Actually Are, the Universal Centrality Rule, Why Singularities Cannot Form, and Why Hawking Radiation Doesn't Exist. BFUT Paper 28. Zenodo. DOI: 10.5281/zenodo.20740461